The mineralogy, geochemistry, and redox state of multivalent cations during the crystallization of primitive shergottitic liquids at various fO_2. Insights into the fO_2 of the martian mantle and crustal influences on redox conditions of martian magmas. C.K. Shearer[1], A.S. Bell[1], P.V. Burger[1], J.J. Papike[1], J. Jones[2], L. Le[2], and N. Muttik[3]. [1]Institute of Meteoritics, University of New Mexico, Albuquerque, NM 87131, [2] NASA Johnson Space Center, Houston, TX 77058. [3]Institute for Advanced Materials, Louisiana State University, Baton Rouge, LA.

Introduction: The fO_2 of crystallization for martian basalts has been estimated in various studies to range from IW-1 to QFM+4 [1-3]. A striking geochemical feature of the shergottites is the large range in initial Sr isotopic ratios and initial ε^{Nd} values [e.g. 1-5]. Studies by [1,2] observed that within the shergottite group the fO_2 of crystallization is highly correlated with these chemical and isotopic characteristics with depleted shergottites generally crystallizing at reduced conditions and enriched shergottites crystallizing under more oxidizing conditions. More recent work has shown that fO_2 changed during the crystallization of these magmas from one order of magnitude in Y980459 (Y98) [6] to several orders of magnitude in Larkman Nunatak 06319 [7]. These real or apparent variations within single shergottitic magmas have been attributed to mixing of a xenocrystic olivine component [2], volatile loss-H_2O disassociation, auto-oxidation during crystallization of mafic phases [7], and assimilation of an oxidizing crustal component (e.g. sulfate) [8]. In contrast to the shergottites, augite basalts such as NWA 8159 are highly depleted yet appear to be highly oxidized (e.g. QFM+4). As a first step in attempting to unravel petrologic complexities that influence fO_2 in martian magmas, this study explores the effect of fO_2 on the liquid line of descent (LLD) for a primitive shergottite liquid composition (Y98). The results of this study will provide a fundamental basis for reconstructing the record of fO_2 in shergottites and other martian basalts, its effect on both mineral chemistries and valence state partitioning, and a means for examining the role of crystallization (and other more complex processes) on the petrologic linkages between olivine-phyric and pyroxene-plagioclase shergottites.

Experimental and Analytical Approach: A series of 1-atmosphere equilibrium experiments on Y98 bulk compositions were performed in Deltech furnaces at the Johnson Space Center and the Institute of Meteoritics (IOM-UNM) at the University of New Mexico. Several overlapping experiments were carried out at both labs to confirm the reproducibility of the experiments. Oxygen fugacities were controlled using CO-CO_2 gas mixtures and sample loop compositions were changed to accommodate experiments at different fO_2. Temperatures of the experiments ranged from 1000°C to 1450°C. The experiments were carried out at fO_2 ranging from IW-1 to QFM+2. Experimental charges were taken above the liquidus to 1470°C and rapidly dropped down to the final experimental temperature. We also conducted several reversal experiments near the liquidus and near temperatures of pyroxene stability. Another subset of experiments was conducted on liquid compositions derived from 1200°C experiments to better determine the stability of plagioclase at temperatures between 1100°C and 1000°C. Thin sections of the experiments were initially examined and documented using backscattered electron imaging on the JEOL JXA-8200. Quantitative point analyses were conducted on various silicates and oxide phases using the electron microprobe. These analyses employed an accelerating voltage of 15 kV, a beam current of 20 nA, and a spot size from 1-3 µm. Chromium and vanadium K-edge XANES data were acquired with the X-ray microprobe of GSECARS beamline 13-ID-E at the Advanced Photon Source (APS), Argonne National Laboratory, Illinois. The beam was focused to a final spot size of 5µm by 5µm [6].

Results:

Liquid lines of descent: The LLD were determined for fO_2 of IW-1, IW, IW+1, IW+2, QFM, QFM+1 and QFM+2. Several intermediate fO_2 experiments were also run. LLD change over this wide range of fO_2:

IW-1: olivine→opx→"spinel"→ cpx→plagioclase

IW+1: olivine→"spinel"→opx→ cpx→plagioclase

QFM: olivine+"spinel"→opx→cpx→plagioclase

QFM+2: "spinel"→olivine→opx→cpx→plagioclase

The liquidus temperatures do not dramatically change and are approximately 1410°C over the range of fO_2. Opx crystallizes at a lower temperature at IW-1 (1250°C) than at more oxidizing conditions (≈1300°C). All melts become saturated with plagioclase at temperatures below 1100°C.

Mineral chemistries: While we still are documenting mineral chemistries at the liquidus, here we compare and contrast phase compositions in constant temperature experiments at different fO_2 and constant fO_2 experiments at different temperatures. "Spinel" exhibits the most dramatic change in composition (see [9,10] for details). The "spinel" is dominated by the chromite component. With increasing fO_2 at any one temperature, the magnetite component, $Mg/(Fe^{2+}+Mg)$, and the chromite/spinel ratio all increase. The most dramatic increases in the magnetite component are at fO_2 values more

oxidizing than IW+2. At QFM+2, the magnetite component increases up to 25 mol. %. This observation is of considerable importance as this composition of the "spinel" never approaches that of end-member magnetite. With decreasing temperature the chromite/spinel and the $Mg/(Fe^{2+}+Mg)$ decrease.

At IW-1, the first observation of olivine is in the 1400°C experiments with a composition of Fo_{76}. Based on melt composition and mass balance we believe that small quantities of olivine crystallize at slightly higher temperatures (1410-1420°C), but we were unable to document these small modal abundances. By 1200°C the olivine composition is Fo_{70}. In contrast, at QFM+2 the first olivine crystallizes at approximately 1380°C with a composition of Fo_{85}. By 1200°C the olivine composition is Fo_{77}. The olivine to crystallize from IW+1 experiments at 1400°C has a composition of Fo_{81}. In Y98, the olivine cores have compositions that approach Fo_{86}.

At IW-1 the pyroxene that appears in the ≈1200°C has a composition of approximately $En_{68}Wo_6$ with a Fe^{3+}/(total Fe)=0.00. At more oxidizing conditions (QFM+2), the pyroxene that appears in the 1200°C has a composition of approximately $En_{75}Wo_{2.8}$ with a Fe^{3+}/(total Fe)=0.09. Near the first appearance of opx in these experiments, the pyroxene composition is $En_{79}Wo_2$. In Y98, the opx cores have a composition of $En_{80}Wo_2$.

Melt composition: The Mg# of melts predictably decrease with both decreasing temperature and decreasing fO_2. The effects of fO_2 are particularly apparent at conditions more oxidizing than FMQ. Titanium, Ca, and Al are incompatible along LLD until temperatures fall below 1200°C. The concentrations of these elements begin to decrease in the melt as pigeonite, plagioclase, and more Ti-rich spinel become stable along the LLD. In particular, the presence of spinel appears to have a more substantial effect on Ti at higher at higher fO_2 than is observed for more reducing conditions.

Valance state: We measured or calculated the valance state of Fe in melt (and its effect on Fe in plagioclase) and for both V and Cr in melt and olivine during the equilibrium crystallization of Y98. Initially using the relationships between $Fe^{3+}/\Sigma Fe$ and fO_2 [11,12], we estimated the variation in $Fe^{3+}/\Sigma Fe$ at different fO_2 during crystallization. Just below the liquidus, the $Fe^{3+}/\Sigma Fe$ is approximately 0.0 at IW-1 and increases to 0.05 at IW+2. $Fe^{3+}/\Sigma Fe$ increases to 0.10 at QFM, 0.22 at QFM+2, and 0.35 at QFM+3 (Fig. 1). Iron in plagioclase reflects this changing fO_2 as Fe^{3+} is strongly preferred in plagioclase compared to Fe^{2+} [13,14]. Using Fe concentrations for fractionated Y98 melts (at 1100°C) D values from [14], and iron as calculated as Fe_2O_3, the Fe_2O_3 in late-stage plagioclase increases from 0.55 at IW-1 to 0.75 at QFM, to 1.8 at QFM+2 (Fig. 1). Variation in $Cr^{2+}/\Sigma Cr$ at 1200°C in olivine is also illustrated in Fig. 1. These values in olivine directly reflect the variation in the melt [6]. The $Cr^{2+}/\Sigma Cr$ in olivine is also temperature dependent, this value increases approximately 6% for every 100°C from 1200°C to the liquidus temperature. Along LLD at different fO_2 the behavior of V is controlled by its redox state (V^{3+}, V^{4+}, V^{5+}), the relative stability of olivine and the "spinel", and the spinel composition.

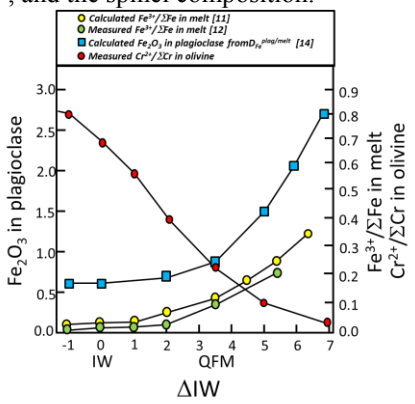

Fig1. Variation in multi-valent cations with fO_2 in Y98.

Initial application of results: These experimental results have direct application for interpreting the origin and evolution of martian basalts. For example: (1) As earlier illustrated by [15] and presented in much more detail here and in [9], early spinel and silicate compositions systematically reflect the fO_2 under which primitive martian basalts crystallize. (2) Spinel compositions that crystallize from primitive magmas such as Y98 at extremely high fO_2 have a substantial magnetite component. However, end-member magnetite has not been observed as a magmatic phase. (3) LLD and evolving martian melt compositions are distinct at different fO_2. Significant difference occurs at conditions more oxidizing than QFM. These data provide a baseline for interpreting more complex processes linking martian olivine-phyric basalts to more fractionated basalts (e.g. basaltic shergottites, augite basalts).

References: [1] Wadhwa (2001) Science 291, 1527-1530. [2] Herd et al., (2002) GCA 66, 2025-2036. [3] Agee et al. (2014) MetSoc 77. [4] Shih et al., (1982) GCA 46, 2323-2344. [5] Borg et al., (2005) GCA 69, 5819-5830. [6] Bell et al. (2015) LPSC 46, abstract #2421. [7] Peslier et al (2010) GCA 74, 4543-4576. [8] Bell et al. (2016) LPSC 47, in press. [9] Burger et al. (2016) LPSC 47, in press. [10] Papike et al. (2015) Am. Mineral. 100, 2018-2025. [11] Kress and Carmichael (1991) Contrib. Mineral Petrol. 108, 82-92. [12] Righter et al. (2013) [13] Lundgaard and Tegner (2004) Contrib. Mineral. Petrol 147, 470-483. [14] Phinney (1992) GCA 56, 1885-1895. [15] McKay et al. (2004) LPSC 35, abstract #2154.